Acoustic backscatter and attenuation due to river fine sediments: experimental evaluation of models and inversion methods

Adrien Vergne[1], Céline Berni[1], Jérôme Le Coz[1], and Florent Tencé[1]

[1]INRAE, UR RiverLy, River Hydraulics, 5 rue de la Doua CS 20244, 69625 Villeurbanne, France

Key Points:

- Acoustic backscatter and attenuation of a homogeneous suspension of fine river sediment were measured in a laboratory tank
- The results of existing models are highly sensitive to particle size distribution uncertainty
- Inversion using both backscatter and attenuation yielded accurate concentration estimates

Corresponding author: Céline Berni, `celine.berni@inrae.fr`

Abstract

The hydroacoustic monitoring of suspended sediment concentration (SSC) in rivers is based on the inversion of backscatter and attenuation models. To evaluate such models, acoustic backscatter and attenuation were measured from a homogeneous suspension of fine river sediments (clay) in a laboratory tank at various concentrations in the range 1-18 g/l. Agreement between the modelled and measured acoustic backscatter and attenuation values was found to be relatively poor. The results are highly sensitive to particle size and shape which come with large measurement uncertainties and can be significantly improved by adjusting plausible particle parameters. Various inversion methods combining single or multiple frequencies, analysis of backscatter and/or attenuation, spherical or oblate shape hypothesis for particles and fixed or estimated lognormal grain size distribution are tested. The most promising inversion methods using both backscatter and attenuation information led to accurate SSC estimates.

1 Introduction

Following the success of the Acoustic Doppler Current Profiler (ADCP) technology for monitoring river discharge, there has been a growing interest in the last decade in extracting information on Suspended Sediment Concentration (SSC) from acoustic backscatter in rivers. One major advantage of using sonar systems such as ADCPs or Acoustic Backscatter Systems (ABSs) for monitoring SSC in rivers is the capacity of these instruments to provide measurements at a much higher spatial and temporal resolution than traditional water sampling techniques. Despite the efforts recently made to find a relation between SSC and acoustic backscatter in rivers (e.g. Gray & Gartner, 2009; Venditti et al., 2016), most studies remain empirical and site-specific. The present work, based on laboratory experiments, intends to contribute to the development of more general methods applicable in rivers.

A bimodal Particle Size Distribution (PSD) is commonly observed in rivers (e.g. Agrawal & Hanes, 2015; Armijos et al., 2017). The first mode is usually composed of silt and clay sediment particles and is often fairly well mixed throughout the river cross-section. The second mode is made of fine to coarse sand particles and it usually presents strong lateral and vertical gradients, with concentration increasing towards the bed. Sonar technology could potentially provide information on both of these modes. However, even when the interest is only in monitoring sand SSC, the impact of fine suspended sediments on the recorded backscatter signal must be assessed.

Thanks to substantial efforts in acoustical oceanography (Sheng & Hay, 1988; Hay, 1991; Hay & Sheng, 1992; Thorne et al., 1993; Thorne & Buckingham, 2004; Thorne & Meral, 2008; Moate & Thorne, 2012), the acoustic response of a suspension of sand particles is now relatively well understood and modelled. Inversion techniques have been developed based on these models, the most powerful ones using multiple frequencies and computing both SSC and particle size along the backscatter profile (see Thorne & Hurther, 2014, for a review). Compared to marine science, the understanding of river suspension backscattering is much less advanced (see Szupiany et al., 2019, for the latest significant advances). In the case of a homogeneous suspension of fine sediment that can often be met in rivers, deploying one instrument horizontally allowed to monitor fine SSC with horizontal ADCPs in rivers, through either empirical approaches (Wright et al., 2010; Moore et al., 2012; Landers et al., 2016; Topping & Wright, 2016) or multi-frequency inversion (Moore et al., 2013). But in situ backscatter data with a calibrated instrument is still needed: 1. to validate existing models and inversion methods for fine sediment and 2. to check whether some unknown calibration value hides significant physical processes (Vergne et al., 2020). Therefore, this work focuses on river fine sediments acoustic properties.

While fine river suspended particles are known to be able to aggregate in flocs, the focus of this study is only on primary, i.e. un-flocculated, particles. The impact of flocculation on acoustic backscattering has been studied by others (MacDonald et al., 2013; Rouhnia et al., 2014; Thorne et al., 2014; Vincent & MacDonald, 2015). The authors of the present study believe that working on primary particles is valuable for river applications, as rivers often show low organic matter, no salinity, and relatively high turbulence during high sediment load events such as floods – making the setting up of large flocs more unlikely (Burban et al., 1989; Droppo, 2001).

The sonar response of suspended sediments is determined by sound backscattering and sound attenuation. The first goal of this study is to test the efficiency of existing backscatter and attenuation models for natural river fine suspended sediments. Then, the second goal of this study is to assess the efficiency of inversion methods designed to retrieve SSC from acoustic signal, in the simplest case where the suspension is homogeneous along the acoustic beam.

To serve the goals of this study, a homogeneous suspension of natural river clay sediment particles was set up in a laboratory tank. The acoustic backscatter and attenuation were measured at various frequencies. The concentration in the tank was gradually increased in the range $\sim$ 1-18 g/l. This range of concentrations was chosen as representative of high to very high SSC observed in rivers. The material and methods for these experiments is presented section 2. In section 3, the data are compared to existing backscatter and attenuation models in order to review the efficiency of these models. Then, in section 4, four inversion methods are tested, and their outputs are discussed. Conclusions are drawn in section 5.

2 Material and Methods

2.1 Backscatter and Attenuation Models

We consider here a suspension of non-cohesive solid particle. In the monostatic configuration, when acoustic transmitter and receiver are actually the same piston transducer, scatterers of random position lead to an echo signal that is described by the sonar equation:

$$\overline{V_{rms}^2} = \frac{16\pi}{3} \frac{k_t^2 s_v}{\psi^2 r^2} \mathrm{e}^{-4(\alpha_w+\alpha_s)r} \tag{1}$$

where V_{rms} (Volts) is the root mean square of the amplitude of the voltage recorded by the instrument, $\overline{V_{rms}^2}$ is the quadratic average of V_{rms} over a large number of sonar pings, r (m) is the range from the transducer, ψ is a near field correction (Downing et al., 1995), k_t (V.m$^{3/2}$) is a calibration constant specific to the instrument (Betteridge et al., 2008), s_v (m^2.m^{-3}) is the volume backscattering coefficient (Medwin & Clay, 1998) and α_w and α_s (m^{-1}) are the sound attenuation due to water and sediment, respectively. In the following, we will ignore ψ as all the measurements will be made in the far field of the transducers ($\psi = 1$).

Both attenuation and backscattering depend on the suspended sediment concentration and the particles properties. Conventional models are used in this work, considering spherical and oblate particle shapes for attenuation (see Appendix A).

2.2 Inversion Methods

2.2.1 Overview

A number of backscatter model inversion methods to retrieve the SSC from measure backscatter (s_v) have been developed in the last three decades for coastal applica-

tions (Hay & Sheng, 1992; Thosteson & Hanes, 1998; Thorne et al., 2011; Hurther et al., 2011; Wilson & Hay, 2015, among others). These methods were mainly designed for inverting sand suspension SSC profiles. When the suspension can be assumed homogeneous, as is the case of our experiments, the inversion process simplifies substantially, as the sonar equation (eq. 1) becomes explicit.

Two pieces of information (α_s and s_v) per acoustic frequency can be extracted. For example, a single-frequency ADCP can be used in rivers to measure the fine sediment and sand acoustic responses separately (Topping et al., 2007; Wright et al., 2010; Hanes, 2012; Topping & Wright, 2016). When only fine sediments are present, both the SCC and particle size can be retrieved from single-frequency α_s and s_v measurements.

When both backscatter (s_v) and attenuation (α_s) are measured at various frequencies, one can use all this information to retrieve SSC and some other sediment characteristics. To limit the number of parameters to be estimated and keep the inversion methods as robust as possible, the shape of the particle size distribution can be fixed. Generally, we assume a log-normal number particle size distribution:

$$n(a) = \frac{1}{a\sigma\sqrt{2\pi}} \mathrm{e}^{-((\log_\mathrm{e}(\mathrm{a})-\mu)^2/2\sigma^2)} \tag{2}$$

where $n(a)$ is the particle radius probability density function in number of particles, $\mu = \log_e(a_0)$ where a_0 is the median radius of the number PSD, and σ is the scaling parameter. In this case, the sediment characteristics to be estimated are a_0 and σ. These PSD particles parameters are gathered in a variable noted $\boldsymbol{\theta}$, as long as the SSC (M) and other particles parameters such as the spheroid aspect ratio (h) for oblate particles, defined as the ratio between the semi-minor and semi-major axis, when needed.

This choice can be discussed as the PSD encountered in some flows can be significantly different from log-normal, but alike most of the existing inversion methods, we did this standard assumption in most of our inversion methods.

In some cases, we assumed a bimodal distribution for sediments. The PSD is then discribed as follows :

$$\begin{aligned} n(a) \quad = \quad & w_1 \frac{1}{a\sigma_1\sqrt{2\pi}} \mathrm{e}^{-((\log_\mathrm{e}(\mathrm{a})-\mu_1)^2/2\sigma_1^2)} \\ & + (1-w_1) \frac{1}{a\sigma_2\sqrt{2\pi}} \mathrm{e}^{-((\log_\mathrm{e}(\mathrm{a})-\mu_2)^2/2\sigma_2^2)} \end{aligned} \tag{3}$$

$$\mu_1 = \log_e(a_1) \qquad \mu_2 = \log_e(a_2) \qquad 0 \leq w_1 \leq 1$$

where a_1 and a_2 are the mean diameters of the two modes, with respective scaling parameters σ_1 and σ_2 and w_1 the relative weight of the two modes.

In this study, four inversion methods are tested to retrieve the SSC from the acoustic signal, in the simplest case where the suspension is homogeneous along the acoustic beams. The first two were presented in previous articles whereas methods 3 and 4 are introduced in this article. The various implementations tested are summarized in Tab. 1.

Method 1 is taken from Thorne and Hurther (2014). It is representative of the many inversion methods developed in acoustical oceanography for measuring sand suspensions. The inversion algorithm uses backscatter information (s_v) at various frequencies. In implementation M1.1 and M1.2 (see Tab. 1), $\boldsymbol{\theta} = (M, a_0)$ and $\boldsymbol{\theta} = (M, a_0, \sigma)$ are estimated respectively.

Method 2 was proposed by Moore et al. (2013). It was designed for measuring river fine sediment suspensions with uncalibrated ADCPs. The inversion algorithm uses attenuation information (α_s) at various frequencies. In implementations M2.1 and M2.2, $\boldsymbol{\theta} = (M, a_0)$ and $\boldsymbol{\theta} = (M, a_0, \sigma)$ are estimated, respectively, using a viscous attenuation model for spheres. In implementations M2.3, M2.4 and M2.5, $\boldsymbol{\theta} = (M, a_0)$, $\boldsymbol{\theta} = (M, a_0, \sigma)$ and $\boldsymbol{\theta} = (M, a_0, h)$ are estimated, respectively, using a viscous attenuation model for oblate spheroids.

Method 3 uses the ratio of attenuation to backscatter at only one frequency ; $\boldsymbol{\theta} = (M, a_0)$ is estimated. Such method was also applied by Guerrero and Di Federico (2018) and Aleixo et al. (2020).

Method 4 uses both backscatter and attenuation information at various frequencies. Viscous attenuation models for spheres (M4.1 and M4.2) and oblate spheroids (M4.3 and M4.4) are tested. In implementations M4.1, M4.3 and M4.4, $\boldsymbol{\theta} = (M, a_0, \sigma)$, $\boldsymbol{\theta} = (M, a_0, \sigma)$ and $\boldsymbol{\theta} = (M, a_0, \sigma, h)$ are estimated respectively. In implementation M4.2, we assumed a bimodal particle size distribution and $\boldsymbol{\theta} = (M, a_1, a_2, \sigma_1, \sigma_2, w_1)$ is estimated.

The next sections describe the four inversion methods in more detail as well as their various implementations.

2.2.2 Method 1: multi-frequency backscatter inversion

We used the algorithm of Thorne and Hurther (2014), that minimizes the objective function Φ:

$$\begin{aligned} \Phi(\boldsymbol{\theta}) &= \frac{\delta_M(\boldsymbol{\theta})}{M_0(\boldsymbol{\theta})} \\ M_0(\boldsymbol{\theta}) &= \frac{1}{N}\sum_{j=1}^{N} M_{0,j}(\boldsymbol{\theta}) \\ \delta_M^2(\boldsymbol{\theta}) &= \frac{1}{N}\sum_{j=1}^{N} M_{0,j}^2(\boldsymbol{\theta}) - [M_0(\boldsymbol{\theta})]^2 \end{aligned} \tag{4}$$

where $M_{0,j}(\boldsymbol{\theta})$ is the model-computed SSC that matches s_v measurement for the j^{th} frequency, using the particle parameters set $\boldsymbol{\theta}$ in the backscatter model. Here, $\boldsymbol{\theta}(a_0, \sigma)$ are the parameters of the log-normal PSD.

In implementation M1.1 (see Tab. 1), σ is fixed prior to the inversion: only a_0 is inverted along with SSC, similarly to what Thorne and Hurther (2014) did. In implementation M2.2, we also tried to invert σ along with a_0 and SSC. In any configuration, the parameter set $\boldsymbol{\theta}_{\mathbf{min}}$ where Φ is found to be minimal is used to retrieve both PSD and concentration (SSC $= M_0(\boldsymbol{\theta}_{\mathbf{min}})$).

2.2.3 Method 2: multi-frequency attenuation inversion

Moore et al. (2013) attenuation-based method minimizes the objective function Γ:

$$\Gamma(\boldsymbol{\theta}) = \sum_{i=1}^{N}\sum_{j>i}^{N} |M_{0,i}(\boldsymbol{\theta}) - M_{0,j}(\boldsymbol{\theta})| \tag{5}$$

where $M_{0,i}(\boldsymbol{\theta})$ and $M_{0,j}(\boldsymbol{\theta})$ are the model-computed SSCs that match the $\alpha_{s,i}$ and $\alpha_{s,j}$ measurements for the i^{th} and j^{th} frequencies respectively – using particle parameter set

Table 1. Detail of the various implementations of the four inversion methods tested. It includes the PSD model used, either log-normal or bimodal; the viscous attenuation model used, either (Urick, 1948) spherical model or (Richards et al., 2003) oblate spheroid model; the consideration of scattering attenuation, either included or neglected in the model; the objective function used, if any; the parameters fixed prior to the inversion and the inverted parameters.

Inversion method	**Case**	**PSD**	**Viscous att. model**	**Scattering attenuation**	**Obj. func.**	**Fixed parameters**	**Estimated parameters**	**Inverse SSC outputs**
Method 1 multi-freq. based on s_v	M1.1	lognorm.	-	-	Φ	$\sigma = 0.88$	M, a_0	largely underestimated SSC, Fig. 7a
	M1.2	lognorm.	-	-	Φ	-	M, a_0, σ	largely underestimated and scattered SSC, Fig. 7a
Method 2 multi-freq. based on α_s	M2.1	lognorm.	spheres	incl. or negl.	Φ or Γ	$\sigma = 0.88$	M, a_0	underestimated SSC
	M2.2	lognorm.	spheres	incl. or negl.	Φ or Γ	-	M, a_0, σ	underestimated SSC
	M2.3	lognorm.	oblate spheroids	neglected	Φ or Γ	$\sigma = 0.88$ $h = 1/40$	M, a_0	fairly accurate SSC when using Γ obj. func., Fig. 8a
	M2.4	lognorm.	oblate spheroids	neglected	Φ or Γ	$h = 1/40$	M, a_0, σ	good SSC output trend, some very overestimated values
	M2.5	lognorm.	oblate spheroids	neglected	Φ or Γ	$\sigma = 0.88$	M, a_0, h	underestimated SSC
Method 3 single-freq. based on s_v and α_s	M3	lognorm.	spheres	included	-	$\sigma = 0.88$	M, a_0	fairly accurate SSC, Fig. 9a
Method 4 multi-freq. based on s_v and α_s	M4.1	lognorm.	spheres	included	E	-	M, a_0, σ	underestimated SSC, Fig. 11a
	M4.2	bimodal	spheres	included	E	-	M, a_1, a_2, σ_1, σ_2, w_1	underestimated SSC, Fig. 11b
	M4.3	lognorm.	oblate spheroids	included	E	$h \in [1/40; 1]$	M, a_0, σ	fairly accurate SSC, Fig. 11c
	M4.4	lognorm.	oblate spheroids	included	E	-	M, a_0, σ, $h_{\min}$	fairly accurate SSC, Fig. 11d

$\boldsymbol{\theta}$ in the attenuation model. The parameter set $\boldsymbol{\theta_{min}}$ where Γ is found to be minimal is used to retrieve the sediment characteristics and concentration (SSC $= \frac{1}{N}\sum_{i=1}^{N} M_{0,i}(\boldsymbol{\theta_{min}})$). In this study, we also tried to use the alternative objective function Φ (eq. 4) instead of Γ.

Following the work of Moore et al. (2013), we tested both the spherical particle model of Urick (1948) (see Appendix, eq. A10) and the oblate spheroid model of Richards et al. (2003) (see Appendix) for modelling sediment viscous attenuation. Note that the oblate spheroid model requires an extra parameter h known as the particle aspect ratio. When using the spherical model (cases M2.1 and M2.2 in Tab. 1), we tested both options of including or neglecting the scattering attenuation in α_s computation (eq. A8). When using the oblate spheroid model (cases M2.3, M2.4, and M2.5), scattering attenuation was always neglected ($\chi_{ss} = 0$).

In Moore et al. (2013), only a_0 was inverted along with SSC. In the present study, we also tried to invert more parameters, e.g. σ or h as detailed in Tab. 1.

2.2.4 Method 3: single-frequency backscatter and attenuation inversion

In this method (case M3 in Tab. 1), both information on α_s and s_v are used to retrieve SSC and particle size at one frequency. The PSD scaling parameter σ is fixed prior to the inversion. The theoretical ratio of attenuation to backscatter is computed for various a_0:

$$\frac{\alpha_s}{s_v} = \frac{4\pi \int_0^\infty a^2 \big[\chi_{sv}(a) + \chi_{ss}(a)\big] n(a) da}{\int_0^\infty a^2 f_\infty^2(a) n(a) da} \tag{6}$$

Note that this ratio does not depend on SSC. In eq. (6), χ_{sv} is computed from Urick (1948) spherical model (eq. A10) and f_∞ and χ_{ss} are computed from Moate and Thorne (2012) model (eq. A4 and A9, respectively). The value of a_0 that leads to the empirically measured α_s/s_v ratio is then used to retrieve SSC from attenuation (cf. eq. A8):

$$M = \alpha_s \frac{4\rho_s \int_0^\infty a^3 n(a) da}{3 \int_0^\infty a^2 \big[\chi_{sv}(a) + \chi_{ss}(a)\big] n(a) da} \tag{7}$$

2.2.5 Method 4: multi-frequency backscatter and attenuation inversion

In this method, a data set of modelled α_s and s_v values is generated at each frequency for various SSCs and various sets of particle parameters. In practice, the particle parameters set $\boldsymbol{\theta} = (M, a_0, \sigma, h)$ includes PSD parameters, plus the aspect ratio h when using the oblate spheroid model of Richards et al. (2003) for computing viscous attenuation (see Appendix). Inverse SSC and particle parameters ($\boldsymbol{\theta}$) are sought by minimizing the following objective function:

$$\mathrm{E}(\boldsymbol{\theta}) = \sum_{\mathrm{j}=1}^{\mathrm{N}} \left(\mathrm{A_j^2} \left| \frac{\widehat{\alpha}_{\mathrm{s,j}} - \alpha_{\mathrm{s,j}}}{\alpha_{\mathrm{s,j}}} \right|^2 + \mathrm{A_j} \left| \frac{\widehat{\mathrm{s}}_{\mathrm{v,j}} - \mathrm{s}_{\mathrm{v,j}}}{\mathrm{s}_{\mathrm{v,j}}} \right|^2 \right) \tag{8}$$

where $\widehat{\alpha}_{s,j}$, $\alpha_{s,j}$, $\widehat{s}_{v,j}$ and $s_{v,j}$ are the j^{th} frequency modelled and measured sediment attenuation, and the modelled and measured backscatter, respectively. The weighting terms A_j are defined as :

$$A_j = \begin{cases} (f_j/f_0)^3 & \text{if } \alpha_{s,j} > 0.1 \text{ m}^{-1} \\ 0 & \text{if } \alpha_{s,j} \leq 0.1 \text{ m}^{-1} \end{cases} \tag{9}$$

where f_j is the j^{th} frequency in MHz and $f_0 = 1.0$ MHz. Weighting terms A_j were introduced to account for the fact that higher frequencies provide more reliable information than lower ones, because α_s and s_v are greater. In the critical case of a very low attenuation ($\alpha_s < 0.1$ m^{-1}, as observed at low frequency and low concentration), the acoustic information is considered too imprecise to be taken into account, then is removed from the inversion process. More importance is also given to sound attenuation (α_s) than to backscatter (s_v) by weighting α_s information with A_j^2, because α_s is more sensitive to SSC and because an error in α_s measurement will propagate to s_v. These weights do not have a strong physical basis: they were chosen because of their capacity to improve inversion outputs. Obviously, further research on model and measurement uncertainties would help improve these coefficients.

This method was tested in four different implementations (cf. Tab. 1). In case M4.1, a log-normal PSD was used to model the particle size, and the viscous attenuation was computed from Urick (1948) spherical model (eq. A10). In case M4.2, the log-normal PSD was replaced by a bimodal PSD. In case M4.3 and M4.4, viscous attenuation was computed using Richards et al. (2003) oblate spheroid model. As smaller particles tend to be flatter, we set the particle aspect ratio h to a constant value $h_{\min}$ lower than one, that corresponds to flat oblate spheroids, when the particle radius was small ($a \leq 1$ μm) ; and we set $h = 1$ (spheres) for $a \geq 10$ μm. Between these two bounds, we made h increase linearly with a. In case M4.3, the value of $h_{\min}$ for the finer particles (i.e. $a \leq 1$ μm) was fixed prior to the inversion. In case M4.4, the value of $h_{\min}$ was also inverted.

2.3 Experimental Facility

2.3.1 Description of the Experimental Facility

To create a homogeneous suspension with fine river sediments, we used a 1 m^3 tank (Fig. 1) filled with fresh water two days before the start of the experiment, in order to let the water degas. Four submerged pumps and two propeller agitators were fixed on rods into the tank to generate turbulence and keep the sediments in suspension. When needed, the orientation of the submerged pumps could be varied remotely to re-suspend some sediments trapped at the bottom and gently raise the concentration without air injection. Water samples were taken within the tank using a 5 mm pipe connected to a peristaltic pump. Extensive sampling in the tank showed that the PSD and the concentration were fairly homogeneous in space, with an SSC relative standard deviation of 1.5 % between the 12 sampling point locations tested. PSD remained fairly constant in time while SSC was decreasing very slowly ($\sim$ 0.2 g/l/hr). Good suspension homogeneity was therefore achieved during each acoustic measurement ($\sim$ 4 min). Water temperature was continuously recorded and remained constant around 35$\pm$1°C during all the experiment. This high temperature was due to submerged pumps heating. We estimated that the uncertainty of water temperature measurement is 0.1 degree, which leads to approximately 0.5 % uncertainty on the water attenuation.

A multi-frequency ABS Aquascat 1000R was deployed horizontally in the tank using 4 transducers at the same time but spanning 6 frequencies (0.3, 0.5, 1.0, 2.5, 4.0 and 5.0 MHz) using the transducers alternatively. Unfortunately, strong ambient noise as well as strong backward reflections prevented us from using the 0.3 MHz data. In retrospect, this strong ambient noise might come from too small acoustic bin size (5 mm). A tile of ultrasonic absorber was put behind and in front of the transducers in order to reduce unwanted backward reflections at 0.3 and 0.5 MHz and decrease the time of sound dissipation between 2 sonar pings. Ping frequency was set to 8 Hz. In the following, one acoustic measurement refers to the average profile computed in quadratic mean over 2000 or more successive pings. The instrument had been previously calibrated by the manufacturer on a suspension of glass beads following Betteridge et al. (2008) procedure.

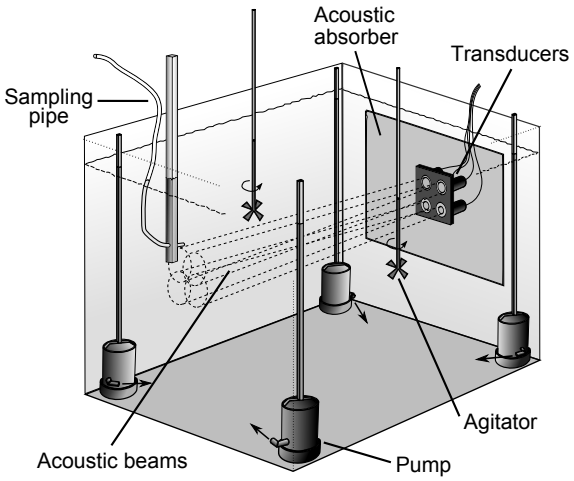

Figure 1. Experimental tank (1m×1m×1m) used in this study. A second tile of acoustic absorber was fixed on the wall facing the transducers (not shown here).

Submerged pumps were producing a relatively small and constant amount of air micro-bubbles. This signal was recorded in clear water prior to the injection of sediments, after letting the pumps run for 1 day. Sensitivity to air micro-bubbles increases with frequency up to 1.0 MHz and decreases thereafter. Overall, air micro-bubble acoustic backscatter was found to be relatively weak, with a Signal to Noise Ratio (SNR) below 10 most of the time. The SNR was computed as the ratio of the basckscatter signal to the ambient noise signal recorded without pulse emission. Sound attenuation due to air micro-bubbles was found to be negligible compared to sediment attenuation.

Wet sediments were injected step by step from the free surface in order to increase the concentration progressively. Freshwater was also added at the end of the experiment to dilute the concentration. We waited for one night between each injection/dilution and the successive acoustic measurements to let the temperature and micro-bubble concentration stabilize. At the very end of the experiment, we did additionnal acoustic measurements as the pumps were turned off, to study lower concentrations and smaller suspended particles. These data were excluded from specific analysis requiring constant PSD data.

2.3.2 Sediment Particles Characterisation

We used natural river sediments collected from a deposition area upstream of the lock of Belley in the Rhône River, France. The sediments were mainly clay, with a small fraction of silt (median diameter $D_{50} \approx 15$ μm, with 10 % of the particles in mass being larger than $D_{90} \approx 40$ μm). They were sieved at 500 μm prior to the experiment to remove coarse organic matter. A Cilas 1190 laser grain-sizer was used to measure the PSD because of the capacity of laser diffraction technology to measure small particles (down to ~ 1 μm). Ultrasounds were applied to the samples before the measurements in order to break potential flocs and have access to the primary particle size. To convert the PSD from volume density $n_v(a_i)$ as given by a laser grain-sizer to number density $n(a_i)$ as needed for acoustic models, we assumed a statistically spherical shape of the particles and used the relation:

$$n(a_i) = \frac{1}{\Delta a_i} \frac{n_v(a_i)/a_i^3}{\sum_i n_v(a_i)/a_i^3} \tag{10}$$

where a_i (m) is the radius of the i^{th} size class of the laser grain-sizer and $\Delta a_i = a_{i+1} - a_i$.

As expected for natural fine sediments, the particles were far from being spherical however. A large diversity in shape was observed when looking at particles collected from the tank suspension with a scanning electron microscope (SEM, Fig. 2). Small clay particles look like fine and flat platelets (Fig. 2a) while bigger particles (> 10 μm) are more similar to angular and irregular polyhedrons (Fig. 2b). The definition and the measurement of one single parameter for describing the size of highly irregular particles is challenging. Even if this problem was circumvented with the assumption of statistically spherical, randomly oriented particles, large uncertainties could come out in the micron and sub-micron ranges when measuring PSD by laser diffraction (Eshel et al., 2004). Comparing Cilas 1190 measurements with a Malvern Mastersizer 2000 on some samples, we found an almost equal D_{50} but somewhat different PSD shape (not shown here). A detailed discussion on particle sizing is out of scope of this paper, but this illustrates the difficulties for precisely measuring the PSD in the case of small particles.

Assuming a spheroidal shape instead of a spherical shape for the particles could help to better take into account the specific shape of fine particles. Indeed, as shown by Schaafsma and Hay (1997), in a spherical approximation, the particle equivalent radius can relate to different quantities depending on the physical process that is considered. When converting mass or volume concentration to number of particles, particle radius relates the radius of a sphere having the same volume as the particle. When considering scattering processes as backscattering and scattering attenuation, particle radius relates to the radius of a sphere having the same geometrical cross-section. Finally, when looking at viscous attenuation, particle radius relates to the radius of a sphere having the same outer surface. These different definitions illustrate the complexity of determining a single "particle equivalent radius" for highly non-spherical particles like fine sediments.

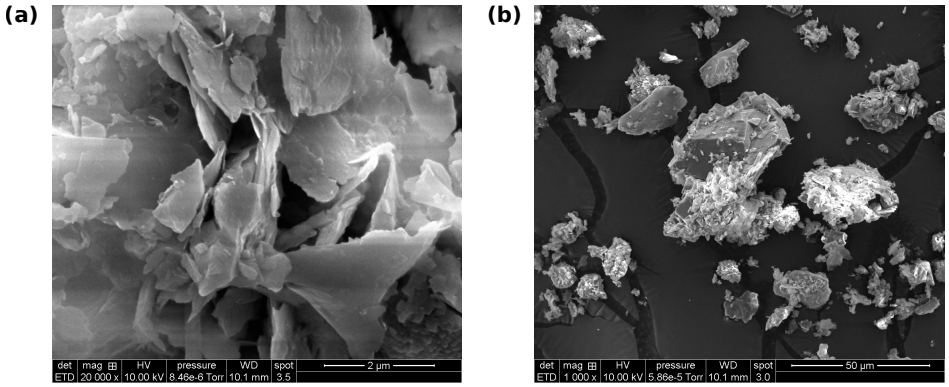

Figure 2. Scanning electron microscope images of suspended sediment particles collected from the tank: (a) small clay platelets, (b) bigger angular silt particles.

Suspended sediment mass concentrations were estimated by filtering the water samples using 0.45 μm glass fiber filters. The uncertainty of this method for the concentrations observed in the tank is estimated to ± 5 %.

For each acoustic measurement, four water samples were taken in the tank within the acoustic beams: two samples at $\sim$ 30 cm from the transducers and two samples at $\sim$ 60 cm. For each location, one sample was used to estimate the SSC, and the other was used to estimate the PSD. We did not observe any significant difference in SSC nor PSD between the two sampling locations so we took the average as the final measured value.

Sediment density in general, and clay density in particular, may deviate from the typical value of 2650 kg.m^{-3} used in many studies. For instance, in a study of numerous soil samples, Schjønning et al. (2017) found a mean clay density of 2886 kg.m^{-3}. Unfortunately, we were not able to measure ρ_s in the present study. Sediment density plays a role at various stages in acoustic modelling. First, it allows to compute the number of particles per unit volume from SSC and PSD. This is the reason why ρ_s appears in equations A2, A3, A7 and A8. Sediment density also plays a role in the viscous attenuation theoretical models (spherical or oblate spheroid), as viscous attenuation is related to the inertia of the particles that depends on their mass. Finally, sediment density also plays a role in the scattering processes (backscatter and scattering attenuation) but in conjunction with other properties of the particle material like compression and shear wave velocities (Gaunaurd & Uberall, 1983). Moate and Thorne (2012) backscatter and scattering attenuation semi-empirical models (eq. A4 and A9) already account for some particle material variability, that is, the models were fitted to experimental data using sand particles of various material. In the following, we assume the sediment density to be equal to 2650 kg.m^{-3} and test the sensitivity to this assumption.

2.3.3 Attenuation and Backscatter Measurements

For each acoustic measurement averaged over many sonar pings as explained in section 2.3.1, the sediment attenuation coefficient (α_s) was estimated using the Fluid Corrected Backscatter (FCB):

$$\mathrm{FCB} = \frac{1}{2}\log_{\mathrm{e}}\left(\frac{16\pi}{3}\mathrm{k_t^2\,s_v\,e^{-4r\alpha_s}}\right) \tag{11}$$

For a homogeneous suspension, $k_t^2 s_v$ is constant along the acoustic path and α_s is given by the FCB slope:

$$\alpha_s = -\frac{1}{2}\frac{\mathrm{dFCB}}{\mathrm{dr}} \tag{12}$$

Fig. 3a shows an example of FCB profiles measured during the experiments, with the intercepts set to 0 for $r = 0$ in order to make the slope comparison easier. The FCB varies fairly linearly with range r, which confirms the suspension homogeneity.

The volume backscattering coefficient (s_v) was estimated with eq. (1) using the empirical value of α_s obtained from eq. (12). Fig. 3b shows an example of s_v profiles measured during the experiment. As expected for a homogeneous suspension, s_v is fairly constant with range. In the following, s_v will be averaged along the acoustic profile.

We were not able to measure s_v for frequencies lower than 1.0 MHz due to the very weak target strength of fine sediments at low frequency compared to the noise level. As small particles produce weak backscatter and strong attenuation, the measurements were very sensitive to noise issues. We observed noise influence for SNR lower than 10, a threshold consistent with other studies using sonar (e.g. Gostiaux & van Haren, 2010). Note that noise issues related to fine sediment low backscatter signal are also encountered in field deployment (e.g. Haught et al., 2017).

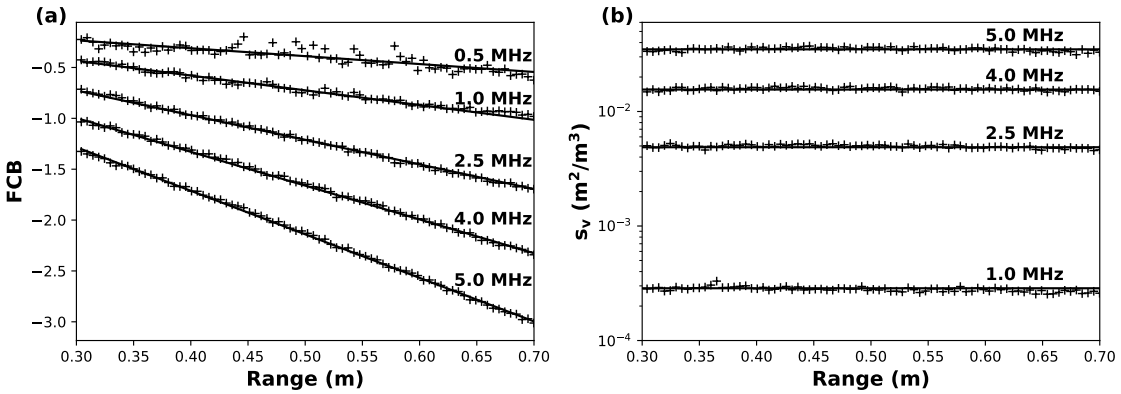

Figure 3. Example of profiles (crosses) with linear fit recorded in the tank for $M \approx 9.5$ g/l: (a) fluid corrected backscatter (FCB); (b) volume backscattering coefficient (s_v). The intercepts of the FCB profiles were set to 0 for $r = 0$ to make the slope comparison easier

Because air micro-bubbles had negligible influence on attenuation, we estimated α_s provided that the recorded backscatter signal was sufficiently strong compared to the ambient noise signal. Therefore, α_s was estimated for all the acoustic profiles or part of the acoustic profiles where $\mathrm{SNR_{amb}} = \overline{V_{rms}^2} \,/\, \overline{V_{amb}^2} > 10$, where $\overline{V_{amb}^2}$ is the ambient noise recorded in the tank without sonar ping emission. Conversely, air micro-bubbles signal could potentially affect s_v measurements. To overcome this problem, s_v was estimated only for range cells where $\mathrm{SNR_{bub}} = \overline{V_{rms}^2} \,/\, \overline{V_{bub}^2} > 10$, where $\overline{V_{bub}^2}$ is the bubble backscatter signal recorded in clear water prior to sediment injection.

2.3.4 Attenuation and Backscatter vs. SSC

Fig. 4a shows the relations between SSC and α_s in the tank at various frequencies. As predicted by the theory when multiple scattering can be neglected and as observed in numerous other studies (e.g. Urick, 1948; Hay, 1991; Sung et al., 2008; Hunter et al., 2012; Moore et al., 2012; Rice et al., 2014, among others), there is a good linear relation between sound attenuation and sediment concentration (cf. Tab. 2). Linear relations between s_v and SSC are not as good however (Fig. 4b, Tab. 2). This is probably due to the very small target strength of fine sediments, making the precise measurement of their backscatter more challenging. In addition, s_v is particularly sensitive to the largest particles in suspension. Gradual deposition of these particles might impact s_v while negligibly impacting SSC and PSD as these particles represent a small volume compared to the total volume of the suspended particles. Note that as the pumps were turned off at the very end of the experiment – which corresponds to SSC < 3 g/l (grey points) in Fig. 4 – particle size decreased and it modified the slope of the relations of α_s and s_v to SSC. Therefore, dashed regression lines in Fig. 4 as well as the values presented in Tab. 2 have been computed excluding these variable PSD data (see Fig. 6). Note also that the slopes of the relation of s_v to SSC for the different frequencies should be linearly related (with a slope equal to 4) in the Rayleigh regime. This is not what we observed, most probably because of the uncertainty in s_v determination for such fine sediment and because we did not considered a single grain size but poorly sorted sediment with a wide PSD.

The values of the attenuation to SSC slopes presented in Tab. 2 are consistent with other similar river sediment studies (e.g. Moore et al., 2012, Tab. 4). Note that sediment attenuation not only presents a better linear relation with SSC (higher R^2), but is also ~ 100 times more sensitive to fine SSC than s_v is. For these reasons, sound attenuation

is a better proxy than backscatter for calibrating an ABS or an ADCP in relation to fine SSC. This type of calibration is more effective when using high frequencies, as the sensitivity to SSC increases while the uncertainty in the determination of FCB slope decreases. Such calibration is however very sensitive to any change in the particle characteristics, and particularly in the PSD as confirmed by the grey points that deviates from this linear relation.

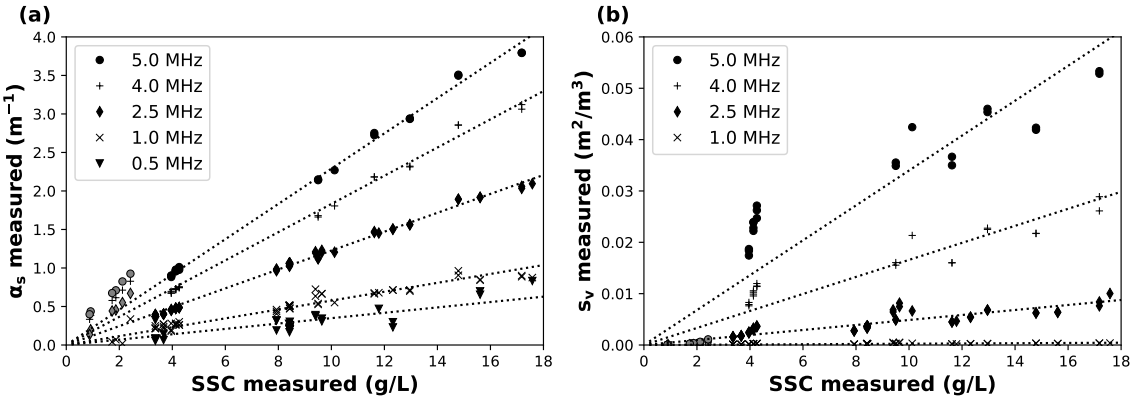

Figure 4. Measured SSC vs. (a) measured sediment attenuation (α_s) and (b) range-averaged measured volume backscattering coefficient (s_v). Dashed lines are regression lines forced to the origin computed for constant PSD data. Grey points indicate that the pumps were turned off in the tank and correspond to different PSD.

Table 2. Linear relation (R^2 and slope with 95 % confidence interval) of attenuation (α_s) vs SSC and backscatter (s_v) vs SSC, computed for SSC > 3 g/l in the experimental tank

	Attenuation		Backscatter	
Frequency	$\mathbf{R^2}$	**slope** ($\mathbf{l.g^{-1}.m^{-1}}$)	$\mathbf{R^2}$	**slope** ($\mathbf{l.g^{-1}.m^{-1}}$)
0.5 MHz	0.63	0.035 ± 0.001	-	-
1.0 MHz	0.95	0.058 ± 0.002	0.60	$0.02 \pm 0.003 \times 10^{-3}$
2.5 MHz	0.99	0.123 ± 0.003	0.81	$0.49 \pm 0.032 \times 10^{-3}$
4.0 MHz	0.99	0.183 ± 0.003	0.91	$1.66 \pm 0.11 \times 10^{-3}$
5.0 MHz	0.99	0.229 ± 0.005	0.87	$3.40 \pm 0.26 \times 10^{-3}$

3 Acoustic Model Performances

3.1 Evaluation of Acoustic Model Outputs

Acoustic model output are compared to the measurements (cf. Fig. 5). The theoretical α_s and s_v from the equations presented in Appendix were computed from the SSC and PSD data measured from water samples. Acoustic modelling was performed using the SSC and PSD associated to each acoustic measurement, so that variations of PSD at low concentrations (SSC < 3 g/L, pumps off) are taken into account.

Overall, the attenuation modelled using Urick (1948) spherical model is ~ 35 % lower than the measurements (Fig. 5a). This value is consistent with the field study of Haught et al. (2017). Conversely, the modelled backscatter is dramatically overestimated by a factor 4.8 (Fig. 5b). Besides the acoustic models themselves, numerous factors can play a role in these discrepancies. Some of these factors are explored in the next sections.

3.2 Sensitivity to Particle Size and Shape

Applying previous work of Richards et al. (2003) (see Appendix), we were able to compute the viscous attenuation for oblate spheroids instead of spheres. The aspect ratio of the spheroids was set to 1/40 as this value was used in other similar studies (Richards et al., 2003; Moore et al., 2013). For scattering attenuation, we assumed that the total scattering cross-section of an oblate spheroid of semi-major axis a' is equal to the total scattering cross-section of a sphere of radius a'. For both computations we also assumed that the output length of the volume probability density function measured with the laser diffraction is the semi-major axis, which is supported by previous work of Erdoğan et al. (2007). Results for modelled attenuation are greatly improved when using the oblate spheroid model instead of the spherical model (compare Fig. 5a and 5c). Unfortunately, as far as the authors know, there is no available model for backscattering suitable for such fine and plate particles so that we were not able to improve s_v results.

To test the sensitivity of the acoustic models to PSD, we searched for a PSD that would improve the agreement between acoustic modelling and measurements. For a measured SSC, we computed α_s and s_v for a set of automatically generated PSDs. As all the reasonably possible PSDs could not be tested, the following simple procedure was applied: 1. the mean PSD measured by laser diffraction for SSC > 3 g/L (pumps on ; stable PSD in the experimental tank) was fitted with a 3-mode Gaussian mixture model (cf. Masson et al., 2018, for a description of the method); 2. We build new 3-mode Gaussian mixture PSDs with the following characteristics. We sampled mode centres ranging ± 50 % from the three initial (laser diffraction) values. We made the weights of the three mode vary from 0 to 1. The scaling parameters (σ) of the three modes were not changed to keep the computational time reasonable. A set of $\sim 6.5 \times 10^4$ PSDs were generated following this method. Both spherical and oblate spheroid models were used for computing viscous attenuation. Fig. 6 shows the two PSDs leading to the best regression slopes, that is closest to 1, between the acoustic model outputs (α_s and s_v) and the measurements for viscous attenuation computed using the spherical model and the oblate spheroid model, respectively. In both cases, using the "best" PSD obtained from the sensitivity test instead of the PSDs measured by laser diffraction greatly improved model performances as shown in Fig. 5d and 5e. Compared to the mean PSD measured by laser diffraction ($D_{50} = 15\,\mu$m), the "best" PSDs obtained from the sensitivity test are finer ($D_{50} = 7\,\mu$m for the spherical model; $D_{50} = 3\,\mu$m for the oblate spheroid model, cf. Fig. 6). Therefore, the discrepancies between model outputs and measurements (cf. Fig. 5a and 5b) may be due to particles actually finer than what laser diffraction measured, as also observed by Erdoğan et al. (2007).

3.3 Sensitivity to Sediment Density and Flocculation

Acoustic models results depend on sediment density. As a scattering model suitable for silt and clay particles is lacking, we were not able to test the influence of density variations on s_v. However, using Urick (1948) spherical model to compute viscous attenuation and Moate and Thorne (2012) model for scattering attenuation, we were able to compute α_s for various values of ρ_s in the range 2000 – 3000 kg.m^{-3}. Best results were obtained for the highest value of ρ_s (3000 kg.m^{-3}), that made α_s underestimation slightly drop from 35 to 31 %. We conclude that a potential error on sediment density estimation cannot explain the large discrepancies observed in Fig. 5a and 5b.

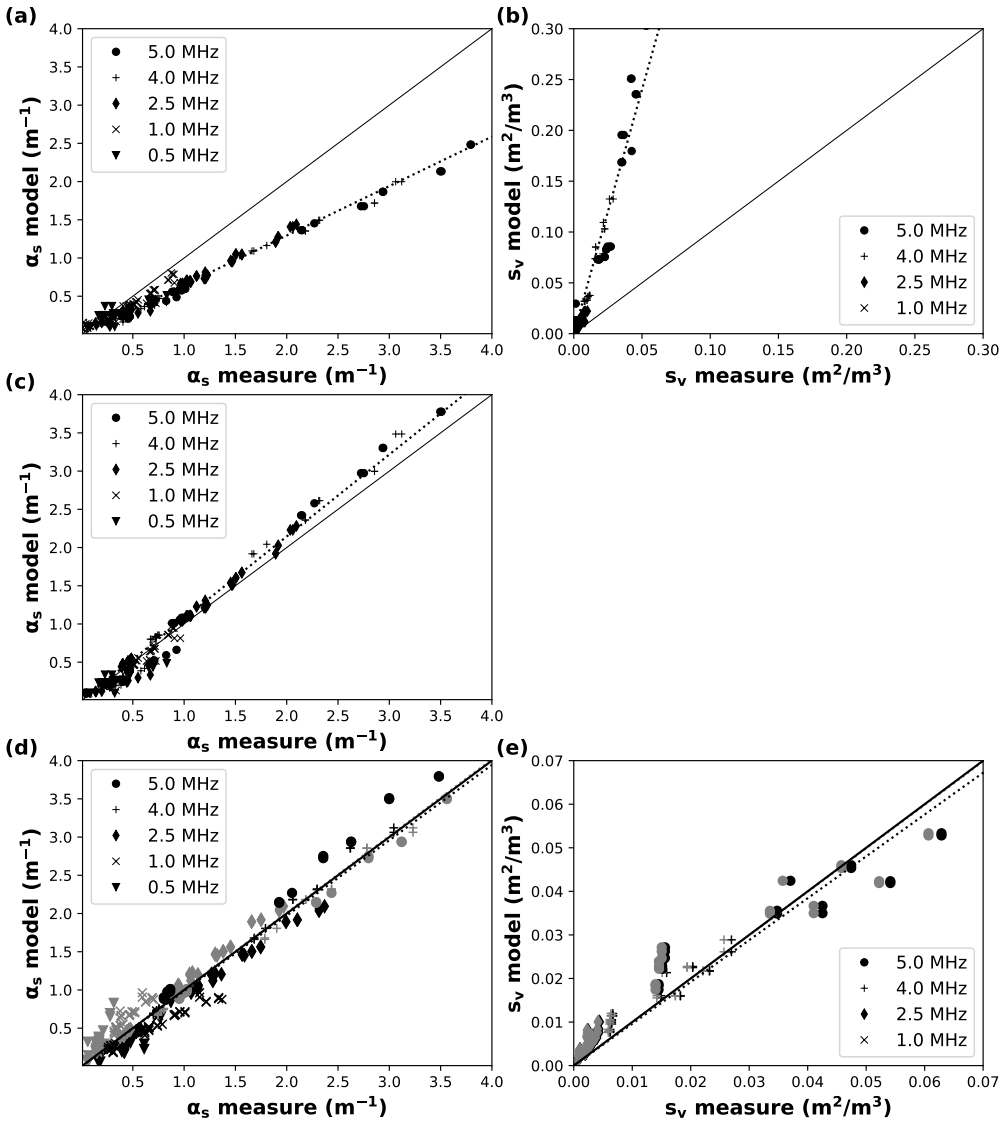

Figure 5. Acoustic model outputs vs. measurements for all available sonar frequencies: (a) sediment attenuation (α_s), PSD data from laser diffraction and viscous attenuation from Urick (1948) spherical model ; (b) volume backscattering (s_v), PSD data from laser diffraction ; (c) sediment attenuation, PSD data from laser diffraction and viscous attenuation from Richards et al. (2003) oblate spheroid model with aspect ratio $h = 1/40$; (d) sediment attenuation, best PSD from sensitivity test, spherical model (black symbols) and oblate spheroid model (grey symbols); (e) volume backscattering, best PSD from sensitivity test, spherical model (black symbols) and oblate spheroid model (grey symbols). Dotted lines are regression lines and solid lines are perfect agreement lines.

Flocculation in the tank was not directly monitored but was certainly negligible, and otherwise, this could not explain the model errors, at least on backscatter s_v. Indeed, first, the high turbulence generated by the pumps and the agitators made the presence of large flocs unlikely. Second, flocculation of fine particles tends to increase the volume backscattering coefficient (s_v) for a given SSC (MacDonald et al., 2013; Rouhnia et al., 2014). For the same mass concentration and same primary particle type, a suspension of flocculated particles leads to larger s_v than a suspension of non-flocculated particles. As ultrasounds were applied to break potential flocs prior to PSD measurement by laser diffraction, the model outputs in Fig. 5a and 5b should relate to the primary particles acoustic response. Hence, the modelled s_v (cf. Fig. 5b) should be even more overestimated if ever flocs were actually formed in the experimental tank.

4 Evaluation of inversion methods

In this section, we show and discuss some outputs of each of the four inversion methods presented in section 2.2 (cf. Tab. 1). The analysis of inversion efficiency is mainly focused on SSC, as this parameter is the most used in river applications, and as SSC is probably the suspension parameter that can be measured with most confidence from water sampling. "True" values of other parameters like particle size are more uncertain, making the comparison with inversion outputs more difficult.

In the following, we sometimes fix the value of the PSD scaling parameter (σ) to 0.88. This value was obtained by fitting a log-normal distribution to the mean volume PSD measured by laser diffraction. Note that for a log-normal PSD, volume and number distributions share the same σ. We also set the particle aspect ratio $h_{\min} = 1/40$ prior to the inversion. We used this value as it was given by Richards et al. (2003) and used by Moore et al. (2013) for similar sediment particles.

4.1 Multi-frequency backscatter inversion (Method 1)

Backscatter is very sensitive to large particles and a change in the PSD scaling parameter (σ) is expected to be a sensitive factor for a backscatter inversion method such

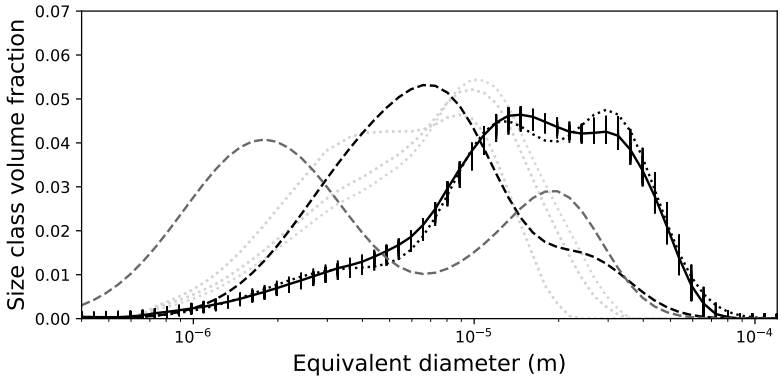

Figure 6. Volume particle size distribution: average of all the laser diffraction measurements (solid black line with error bars including all measurements), excluding the last samples with the pumps off (PSD shown as light grey dotted lines) ; 3-mode Gaussian mixture model fit to the mean PSD (dotted black line) ; PSD sample leading to the best agreement between model outputs (α_s and s_v) and the measurements, using spherical model (dashed black line) or oblate spheroid model (dashed dark grey line) for viscous attenuation.

as M1. We tried both options of fixing it prior to the inversion process (case M1.1 of Tab. 1) and letting it free (case M1.2). In both cases, this inversion method led to quite underestimated SSC outputs (cf. Fig. 7a). When letting σ free, inversion outputs were not only biased but also highly scattered.

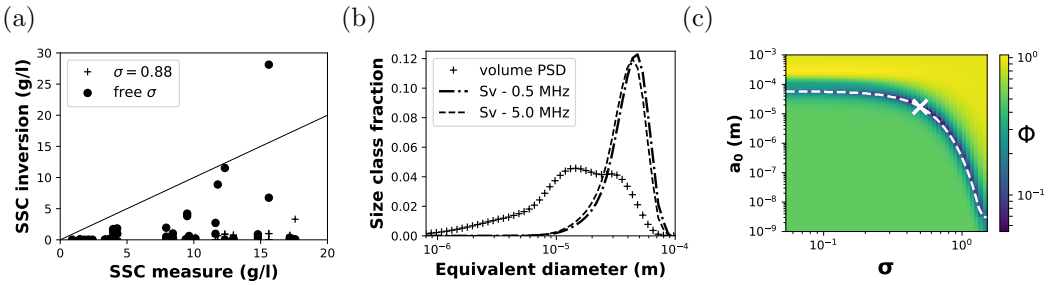

Figure 7. Backscatter multi-frequency inversion outputs (Method 1): (a) inverse SSC vs. measured SSC, in both cases of PSD scaling parameter (σ) fixed prior to the inversion (case M1.1 of Tab. 1) or left free (case M1.2). Solid line is perfect agreement line ; (b) size class volume probability distribution measured by laser diffraction compared to modelled s_v distribution (fraction per size class) at 0.5 and 5.0 MHz ; (c) example of Φ inversion objective function (eq. 4) values in the parameter space (a_0, σ), the white dashed line shows the local minimum valley, the cross indicates the location of the absolute minimum of Φ that is used to retrieve inverse PSD and SSC.

Backscatter-based inversion methods were originally developed and tested on marine sand suspensions. Most often, sand suspensions are well-sorted, i.e. they have a narrow PSD with small σ. For this reason, only one parameter is usually used to describe the particle size, either by considering a single size, or by using a normal or log-normal PSD of fixed σ. For instance, Thorne and Hurther (2014) set $\sigma \approx 0.38$ in their study, that was focused on sand suspension.

Fine sediments often show a much broader PSD. In this case, σ becomes a critical parameter. At common ADCP or ABS frequencies, the backscatter response of fine sediments is likely to be located in the deep Rayleigh regime, i.e. $ka \ll 1$ where k is the wave number and a the particle radius. In this regime, s_v is proportional to $\sim a^3$. Therefore, the right-end of the PSD actually contributes much more to the backscatter than the left-end does. The broader the PSD is, the greater this effect is.

Fig. 7b shows a simulation of the fraction of the total s_v due to each particle-size class at 0.5 and 5.0 MHz, compared to the volume PSD measured by laser diffraction. At 5.0 MHz, 80 % of the backscatter is produced by particles > 30 μm in diameter, although these particles accounts for only ~ 20 % of the total SSC. This illustrates that inversion methods based on backscatter and applied in the deep Rayleigh regime tend to inverse only the right-end of a broad PSD. The inverse PSD is in a way extrapolated from its tail, making the inversion output very sensitive to any small error in the measurements or in the models.

This effect is also illustrated in Fig. 7c, showing an example of Φ objective function (eq. 4) values in the parameter space (a_0, σ). One can see that the minimum values of Φ draw a valley (dashed white line) rather than a single well. Therefore, multiple satisfactory solutions might exist with similar s_v values, but very different inverse SSC.

The inverse a_0 is not very sensitive to σ for narrow PSDs. As σ becomes smaller, the inverse number PSD median diameter $2a_0$ tends to a value close to the peak of s_v probability distribution (~ 50 μm) shown in Fig. 7b. Efficient particles in terms of backscatter should be present for backscatter to be predicted. An error on σ will not affect the inversion outputs strongly in such case. On the contrary, Fig. 7c shows that inverse a_0 becomes very sensitive to σ for wider PSDs. Thus, a small error in fixing σ prior to the inversion may lead to large errors on inverse a_0 and SSC.

We conclude that multi-frequency inversion methods only based on backscatter might not be suitable for suspensions having a broad PSD in the deep Rayleigh regime, which is usually the case for river fine sediments at common ADCP or ABS frequencies.

4.2 Multi-frequency attenuation inversion (Method 2)

Linear relation of attenuation to SSC is less scattered than the relation of backscatter to SSC and overall, better results were obtained with Method 2 than with Method 1.

When using Urick (1948) spherical model (case M2.1 and M2.2), we always found underestimated inverse SSC, even when taking the scattering attenuation into account. This was also observed by Moore et al. (2013).

The best inversion result (cf. Fig. 8a) was obtained from case M2.3 (cf. Tab. 1), using oblate spheroids model and Moore et al. (2013) Γ objective function (eq. 5). When using Φ objective function (eq. 4) instead of Γ, inversion outputs were more scattered. The PSD was log-normal with σ set to 0.88 based on laser diffraction measurement, viscous attenuation was computed using the oblate spheroid model of Richards et al. (2003) with aspect ratio (h) set to 1/40 and the scattering attenuation was neglected ($\chi_{ss} = 0$). Error bars in Fig. 8a show inverse SSC intervals for h in the range [1/80, 1/20] which, as far as we know, could also be plausible. Very similar results were obtained for $h = 1/40$ and $h = 1/80$, while stronger aspect ratios ($h > 1/40$) generally – but not always – led to lower inverse SSC.

The mean inverse D_{50} of the volume PSD found in this configuration was 15.2 μm, which is close to the mean value of 16.0 μm obtained from laser diffraction. However, laser diffraction particle size relates to spherical particle diameter, while acoustic particle size in this case relates to the semi-major axis of oblate spheroids. The drop in the particle size that was measured when the pumps were turned off (cf. Fig. 6), was also retrieved in the inversion results. The fact that the best inversion configuration is closer to real physical conditions (i.e. plate-like particles, broad PSD and realistic particle size) is encouraging. Note that Moore et al. (2013) also found their best results in similar inversion configuration.

When using Richards et al. (2003) oblate spheroid model with free σ (case M2.4), inverse SSC were generally in good agreement with the measurements (regression slope of 1.07 and $R^2 = 0.99$), however some values were highly overestimated (up to ~ 300 %). When letting h free (case M2.5), inverse SSC was underestimated by ~ 50 % and inverse h values were close to 1, which is the aspect ratio of spheres.

As many inversion methods, the method 2 with the Γ objective function basically looks for the point where inverse SSC is the same at all frequencies. This is illustrated graphically in Fig. 8, for two different concentrations. Theoretically, all the curves should meet at one single point, that will provide a_0 and SSC inversion outputs. Fig. 8b shows an example where this theoretical case is well achieved. However, the matching point could sometimes be much more difficult to find, as illustrated in Fig. 8c. Importantly, the Φ objective function detects the smallest relative standard deviation between the curves, while Gamma objective function detects their minimal absolute distance. Thus, Γ will

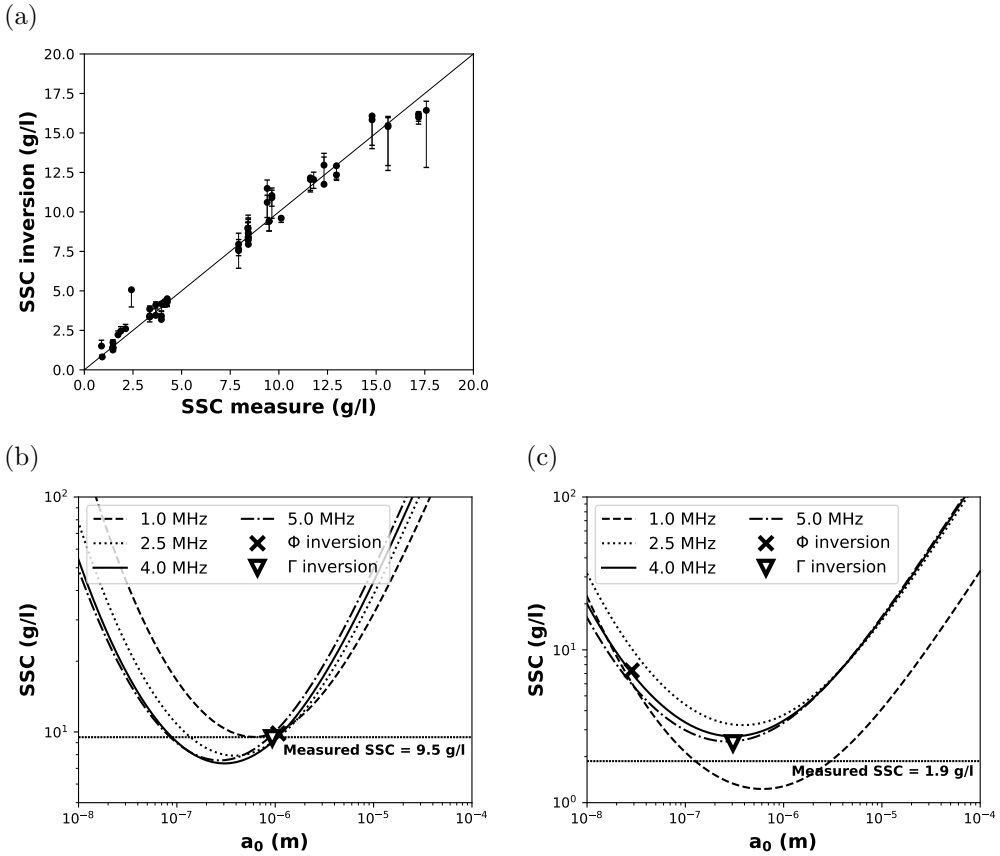

Figure 8. (a) Multi-frequency attenuation inversion outputs (Method 2): inverse SSC vs. measured SSC using the Γ objective function (M2.3, cf. Tab. 1). Error bars show the intervals of inverse SSC for particle aspect ratio (h) in the range [1/80, 1/20]. The solid line shows perfect agreement. (b) and (c) Examples of SSC modelled from measured acoustic attenuation at various frequencies in case M2.3 (cf. Tab. 1) vs the median radius (a_0) of the number log-normal PSD (assumed lognormal) for two different concentrations: (b) SSC = 9.5 g/l ; (c) SSC = 1.9 g/l. Horizontal lines show the measured SSC, crosses and triangles show inversion outputs using Φ and Γ objective functions, respectively.

more likely lead to an inverse a_0 located in the region where the modelled SSC is minimal. In this example, the measured SSC is also located in this region but that may not be the case for a different PSD.

More generally, Fig. 8 illustrates the limits of multi-frequency inversion techniques based on attenuation only. Compared to backscatter (s_v), α_s increases relatively slowly with frequency. When using common ADCP or ABS instruments, only a few frequencies are available, that are relatively low and close to each other. Then, precise measurement of α_s is needed to obtain a clear matching point between the curves at various frequencies as in Fig. 8b example. The inversion efficiency may decrease when the measured attenuation is low, i.e. when SSC is low and/or when using low frequencies. Moreover, the smaller the ratios between the frequencies are, the less accurate this method will be.

We conclude that Method 2 can produce fairly accurate outputs when using Richards et al. (2003) oblate spheroid model. One major advantage of this method is that instru-

ment calibration is not required. However, Method 2 relative success in this study could not be granted for another PSD. Also, two sensitive parameters (σ and h) should be fixed prior to the inversion. This study suggests that laser diffraction measurement could be used to determine σ. Another option would be using calibration data. Method 2 is also sensitive to α_s measurement precision.

4.3 Single-frequency backscatter and attenuation inversion (Method 3)

The Method 3 consists in estimating SSC and median diameter (assuming a log-normal PSD of fixed scaling ratio) using the ratio of attenuation to backscatter at one frequency. Fig. 9a shows Method 3 inversion results with PSD scaling parameter (σ) set to 0.88 (case M3 of Tab. 1). Good agreement was found with SSC measurements, but inversion outputs were more scattered at 1.0 MHz. This is probably due to higher uncertainties in the acoustic measurements, as s_v in particular becomes very small at lower frequencies. The mean D_{50} of the inverse volume PSD varied from 6.4 μm at 5.0 MHz to 9.8 μm at 1.0 MHz. These values are substantially smaller than the value of 16.0 μm obtained by laser diffraction. However, this is consistent with section 3.2 results: when using the spherical model of Urick (1948) for computing viscous attenuation, particle size twice smaller than the PSD measured by laser diffraction leads to better agreement between acoustic modelling and measurements. A one third smaller inverse D_{50} was observed at the very end of the experiment, when the pumps were turned off, which is consistent with the expected drop in particle size.

This method is obviously sensitive to σ parameter. A sensitivity analysis was performed in the range 0.7 - 1.0 for σ. At 5.0 MHz for instance, if σ varies over 0.7-1.0, inverse SSC vary by $\pm$23% (cf. Fig. 9b). Interestingly, this relative error is fairly constant with SSC, since the absolute error becomes smaller as SSC decreases.

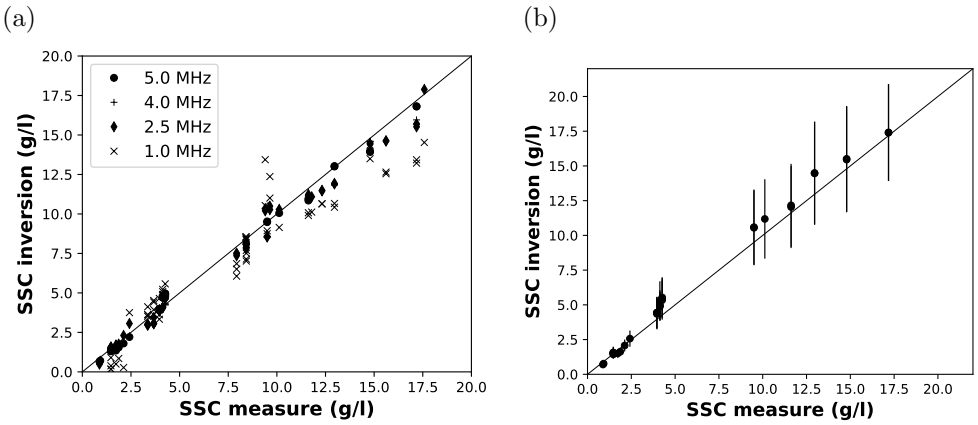

Figure 9. Single-frequency backscatter and attenuation inversion outputs (Method 3): (a) for the various sonar frequencies, with PSD scaling parameter (σ) set to 0.88 ; (b) at 5.0 MHz, inverse SSC mean and range of variation (error bars) for σ varied from 0.7 to 1.0. Solid lines show perfect agreement.

The cause of the relative success of this method is illustrated by Fig. 10, that shows α_s/s_v ratio as a function of the median radius (a_0) of the log-normal PSD, for $\sigma = 0.7$ and $\sigma = 1.0$ at 1.0 and 5.0 MHz. One can see that α_s/s_v ratio is very sensitive to a_0 for fine sediments. This is due to s_v increasing with size while viscous attenuation decreases, leading to a fast drop of α_s/s_v when the particle size increases in the fine sediment mode. When scattering attenuation starts to become dominant, α_s reaches a lo-

cal minimum and starts to increase with size. It makes α_s/s_v increasing slowly up to a constant value in the geometric regime ($\alpha_s/s_v \approx 6$).

We deduce from Fig. 10 that this inversion method should be applied only when viscous attenuation dominates. It approximately corresponds to $\alpha_s/s_v > 10$. For example, this threshold corresponds to a volume PSD D_{50} of ~ 50 μm for $\sigma = 0.7$ at 1.0 MHz, and a volume PSD D_{50} of ~ 10 μm for $\sigma = 1.0$ at 5.0 MHz. Therefore, this inversion method can be suitable, but for silt and clay sediment particles only.

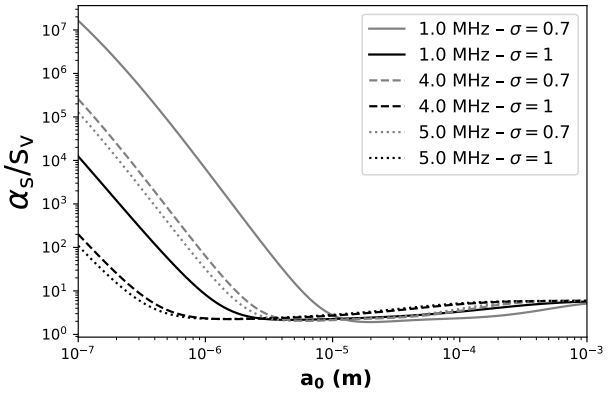

Figure 10. Theoretical ratio α_s/s_v as a function of the median radius a_0 of the log-normal number PSD for $\sigma = 0.7$ and $\sigma = 1.0$ at 1.0 and 5.0 MHz

An interesting feature showed in Fig. 10 is that the slope of α_s/s_v does not change with frequency, i.e. the sensitivity of this method does not depend on frequency. Theoretically, one will prefer using a lower frequency in order to increase the maximum particle size to which the inversion is possible. In practice however, using a lower frequency will make α_s and s_v measurements more uncertain, leading to less precise inversion outputs. The choice of an appropriate frequency might be a trade-off between these two aspects of the problem.

4.4 Multi-frequency backscatter and attenuation inversion outputs (Method 4)

The Method 4 consists in estimating particle parameters (depending on implementation, cf. Tab. 1) using attenuation and backscatter at several frequencies.

Fig. 11a shows Method 4 inverse SSC outputs for case M4.1 of Tab. 1. One can see that inverse SSC is generally underestimated by $\sim 40\%$. Then, considering that attenuation is mainly driven by finer particles and backscatter by coarser ones, we tried to give more freedom to the particle size by using a bimodal PSD (case M4.2). However, besides a much longer computational time, the outputs shown in Fig. 11b were very similar to case M4.1.

We interpret these results as an acoustic model issue: for this experiment at least, there exists a solution (PSD + SSC) that makes the modelled α_s and s_v closer to the measurements than they would be if they were modelled from the real PSD and SSC. In other words, one can better model the acoustic response of the suspension when SSC is set to a value underestimated by $\sim 40\%$. Thus, we expect any (good) inversion algorithm using the same acoustic model to end up with similar results when no prior information is given on the PSD.

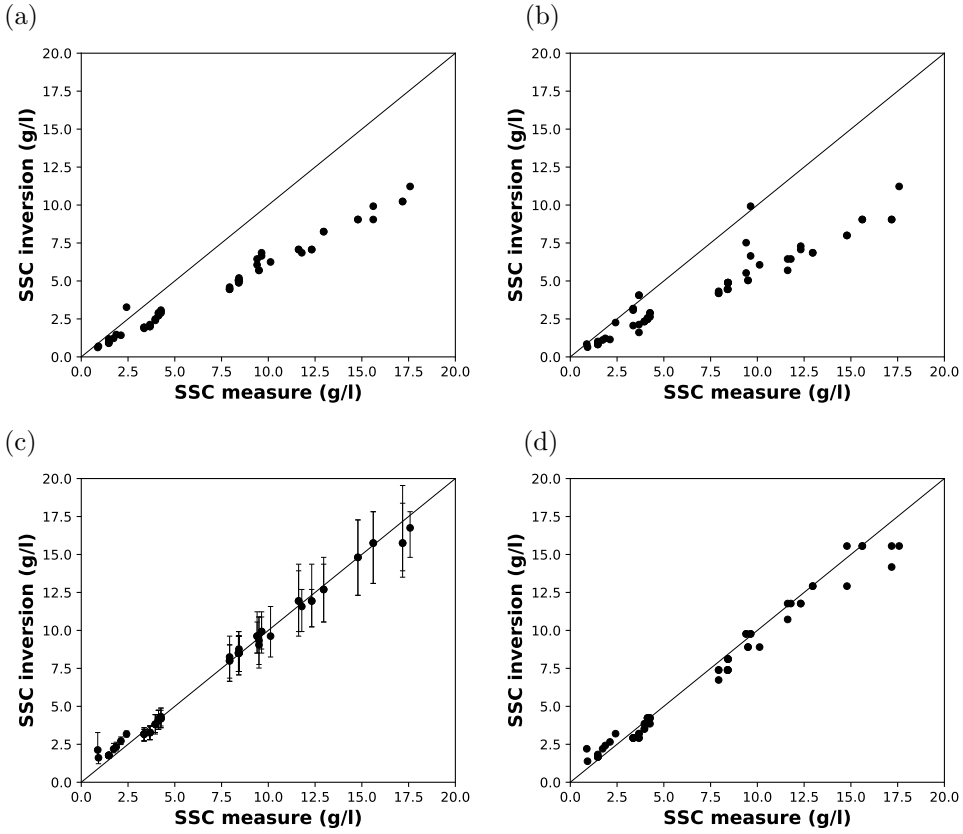

Figure 11. Multi-frequency backscatter and attenuation inversion (Method 4): (a) case M4.1 (cf. Tab. 1), (Urick, 1948) spherical model, log-normal PSD ; (b) case M4.2, spherical model, bimodal PSD ; (c) case M4.3, (Richards et al., 2003) oblate spheroid model, log-normal PSD, minimum particle aspect ratio ($h_{\min}$) set to 1/40, error bars show inverse SSC range for h in the range [1/80, 1/20] ; (d) case M4.4, inverting $h_{\min}$ in addition to PSD parameters and SSC. Solid lines show perfect agreement.

Fig. 11c shows case M4.3 inversion outputs (cf. Tab. 1). Computing viscous attenuation with Richards et al. (2003) oblate spheroid model significantly improves the results, with a mean relative error $< 10\%$.

Finally, Fig. 11d shows inversion outputs obtained when inverting $h_{\min}$ parameter at the same time as a_0, σ and SSC (case M4.4). Inverse SSC values were a little bit underestimated and more scattered than when fixing $h_{\min}$ prior to the inversion, but the mean relative error of $\sim$13% remained fairly acceptable. Inverse $h_{\min}$ values were relatively scattered, but their mean value was $\sim$1/30, which is close to the value of 1/40 provided by Richards et al. (2003) for similar sediment particles.

In both cases M4.3 and M4.4 (Fig. 11c and 11d), inverse σ values were often very close to the upper bound of the inversion range, that was set to 1.2. When reducing or increasing the σ upper bound from 0.7 to 1.3, inverse sigma values remained close to that bound but inverse SSC did not vary substantially. Beyond 1.3, inverse SSC outputs tended to be overestimated and more scattered.

These relatively high σ values led to a relatively small inverse volume PSD mean D_{50} of 3.6 μm for both cases M4.3 and M4.4. For measurements taken when the pumps

were turned off, strong variations in inverse a_0 and σ were observed, without any clear drop in a_0 as expected. The reason why a broader PSD with smaller a_0 better satisfies the inversion optimization process is still unclear.

We conclude that, while this inversion method led to similar SSC outputs as the multi-frequency inversion method (Method 2), it might be less sensitive to the scaling parameter σ as well as the aspect ratio h. In particular, case M4.4 shown in Fig. 11d led to fairly good SSC outputs without specifying the value of neither σ nor $h_{\min}$ prior to the inversion. However, inverse PSD parameters were somewhat unrealistic, with higher σ and lower a_0 than expected.

5 Conclusion

The efficiency of existing acoustic models (for attenuation and backscatter) and inversion methods for fine sediments was evaluated experimentally. We measured the acoustic response of a suspension of fine river particles (with diameters ranging from 1 to 100 μm) at various concentrations in a tank (from 1 to 18 g/L) and computed the theoretical acoustic response using SSC and PSD data from water samples. The agreement between modelled and measured responses was found to be relatively poor, particularly regarding backscatter. However, a simple sensitivity test showed that a PSD finer than the PSD measured by laser diffraction could lead to a much better agreement between models and measurements. This makes it hard to conclude which of the acoustic models or the particle characteristic measurements were wrong. Taking into account the oblate shape of the particles strongly improve the results for attenuation simply considering that the laser diffraction measurement gives the semi-major axis of the spheroids.

River SSC acoustic monitoring would greatly benefit from the development of semi-empirical attenuation and backscatter models for fine sediments, as it has been done in marine science for sand particles. We showed that developing such kind of models requires well-characterized sediment particles, particularly regarding their size. In rivers, organic suspended particles might also explain the uncertainties of existing models and organic content quantification could also be considered (Aleixo et al., 2020), even if in this experiment it was considered as negligible.

While modelling the acoustic response of fine particles is challenging, perfect acoustic models are not always required for efficient signal inversion. In that perspective, four inversion methods were evaluated in this study, in the simplest case of a homogeneous suspension along the acoustic beams.

Backscatter-based inversion method (Method 1) led to unrealistic SSC outputs. Attenuation-based method (Method 2) better succeeded in retrieving SSC, when the right values of σ (PSD scaling parameter) and h (particle aspect ratio) were given prior to the inversion. Indeed, in the deep Rayleigh regime ($ka \ll 1$), sediment attenuation (α_s) provides more information on suspended particles than backscatter.

Combining both attenuation and backscatter information is a promising way of improving inversion techniques. Attenuation to backscatter ratio (Method 3) allowed to accurately invert SSC using only one frequency, when a proper value of σ was provided prior to the inversion. Using multiple frequencies (Method 4) eventually allowed to accurately retrieve SSC without prior assumption on σ or h. However, this led to unexpectedly high inverse σ values, the source of this problem being still unclear. Obviously, the efficiency of these techniques now needs to be assessed through field experiments.

Trying to retrieve suspension characteristics from acoustic measurements using a limited number of frequencies is typically an ill-posed inverse problem, even when using simplified acoustic models. Therefore, one usually needs to fix some suspension parameters prior to the inversion. The remaining free parameters are then inverted. The

applicability of an inversion method in natural environment is a trade-off between the required prior information – that can be missing and/or difficult to estimate – and the precision of the inversion outputs.

The authors believe that this work is a step towards river fine sediment monitoring techniques that would rely less on *in situ* calibration. It claims for the development of multi-frequency and calibrated ABSs suitable for river deployment. Using more and higher frequencies would certainly improve α_s and s_v measurement precision, leading to better inversion outputs. Taking measurement uncertainties into account in the inversion process – for instance using Bayesian inference – also seems to be a promising field of research.

Appendix A Backscatter and Attenuation Models

This section presents an overview of the backscatter theory related to a suspension of non-cohesive solid particles.

A1 Backscatter Models

The volume backscattering coefficient depends on the type and number of scatterers:

$$s_v = \sum_i N_i \sigma_{bs,i} \tag{A1}$$

where N_i (m^{-3}) is the number of scatterers of type i per unit volume and $\sigma_{bs,i}$ (m^2) is their specific backscattering cross-section. For a suspension of solid spherical particles of same radius a (m), material density ρ_s ($\mathrm{kg.m}^{-3}$) and mass concentration M ($\mathrm{kg.m}^{-3}$), equation (A1) becomes:

$$\sigma_{bs}(a) = \frac{a^2 f_\infty^2(a)}{4} \qquad N = \frac{3M}{4\pi a^3 \rho_s} \qquad s_v = \frac{3}{16\pi} K^2 M \tag{A2}$$

where f_∞ is the backscattering form factor and $K = f_\infty(a)/\sqrt{a\rho_s}$ describes the backscattering properties of the particles. When considering a PSD rather than a single size, K is computed over the PSD:

$$K = \left[\frac{\int_0^\infty a^2 f_\infty^2(a) n(a) da}{\rho_s \int_0^\infty a^3 n(a) da} \right]^{1/2} \tag{A3}$$

where $n(a)$ is the particle radius probability density function in number of particles. For a suspension of natural particles, one generally uses an empirical model to compute the form factor. In the following, we applied the semi-empirical model proposed by Moate and Thorne (2012):

$$\frac{f_\infty(a)}{\sqrt{\rho_s}} = \frac{(ka)^2 (1 - 0.25\mathrm{e}^{-[(ka-1.5)/0.35]^2})(1 + 0.6\mathrm{e}^{-[(ka-2.9)/1.15]^2})}{42 + 28(ka)^2} \tag{A4}$$

where k ($\mathrm{rad.m}^{-1}$) is the wave number. This formula has been fitted to marine sand particle suspension data. Note that even when using a semi-empirical backscatter model, a spherical hypothesis is used to convert sediment mass or volume distribution to number of particles.

A2 Attenuation Models

We used the formula of François and Garrison (1982) to compute α_w from water temperature. Attenuation due to particles can be written as:

$$\alpha_s = \sum_i N_i \frac{\sigma_{e,i}}{2} \tag{A5}$$

where $\sigma_{e,i}$ (m^2) is their total extinction cross-section (Medwin & Clay, 1998). For suspended sediments, the two main sources of energy losses are viscous drag and scattering:

$$\sigma_e = \sigma_{sv} + \sigma_{ss} \tag{A6}$$

where σ_{sv} (m^2) and σ_{ss} (m^2) are the total viscous absorption cross-section and the total scattering cross-section, respectively. For spherical particles of radius a, density ρ_s and mass concentration M, the attenuation due to suspended particles is:

$$\alpha_s = \frac{3M}{4a\rho_s}(\chi_{sv} + \chi_{ss}) \tag{A7}$$

where $\chi_{sv} = \sigma_{sv}/(2\pi a^2)$ and $\chi_{ss} = \sigma_{ss}/(2\pi a^2)$ are the normalized viscous and scattering total cross-sections, respectively. When considering a PSD rather than a single size, equation (A7) is computed over the entire distribution:

$$\alpha_s = \frac{3M \int_0^\infty a^2(\chi_{sv} + \chi_{ss})n(a)da}{4\rho_s \int_0^\infty a^3 n(a)da} \tag{A8}$$

Note that when the suspension is not homogeneous but varies with range r along the acoustic profile, α_s needs to be integrated over the propagation path.

To estimate the scattering attenuation, we applied the semi-empirical model of Moate and Thorne (2012):

$$\frac{\chi_{ss}}{\rho_s} = \frac{0.09(ka)^4}{1380 + 560x^2 + 150(ka)^4} \tag{A9}$$

This equation was derived from experimental data in a similar way as equation (A4) form factor.

One generally estimates viscous attenuation using Urick (1948) formula:

$$\begin{aligned} \chi_{sv} &= \frac{2}{3}ka(g-1)^2\left[\frac{s}{s^2+(g+\delta)^2}\right] \\ g &= \frac{\rho_s}{\rho_0} \qquad s = \frac{9}{4\beta a}\left(1+\frac{1}{\beta a}\right) \qquad \delta = \frac{1}{2}\left(1+\frac{9}{2\beta a}\right) \quad \beta = \sqrt{\frac{\omega}{2\nu_0}} \end{aligned} \tag{A10}$$

where $\rho_0 = 1000$ kg.m^{-3}, ω (rad.s^{-1}) is the pulsation and ν_0 is the water kinematic viscosity, set to 0.73 $\times 10^{-6}$ m^2.s^{-1} in this study. Note that this formula was derived from the theory (Urick, 1948; Hay & Mercer, 1989) for the case of spherical particles, but it has been widely applied to natural particles. As far as the authors know, an empirically-based viscous attenuation model for natural particles does not exist yet. However, alternative shape models were derived from the theory, e.g. for oblate spheroids.

The viscous attenuation coefficient α_{sv} for the case of the oblate spheroid model developed by Richards et al. (2003) is expressed in a similar way as eq. (A8) by:

$$\alpha_{sv} = \frac{3M \int_0^\infty a'^2 \chi_{sv}(a') n(a') da'}{4\rho_s \int_0^\infty a'^3 n(a') da'} \tag{A11}$$

where a' is the semi-major axis of the spheroid. The total normalized viscous cross-section χ_{sv} is re-written from Urick (1948) (eq. A10), replacing a by a', and s and δ by:

$$\begin{aligned} s &= \frac{9}{4\beta h a'} K_{sf}^2 \left(1 + \frac{1}{K_{sf}\beta a'}\right) \\ \delta &= L_i + \frac{9}{4\beta h a'} K_{sf}^2 \end{aligned} \tag{A12}$$

where L_i is an inertia factor, K_{sf} is a shape factor and $h = b'/a'$ is the ratio between the semi-minor and semi-major axis of the spheroid, known as the spheroid aspect ratio. L_i and K_{sf} depend on the orientation of the spheroid in relation to the oscillatory motion axis. For oblate spheroids oscillating parallel to their axis of symmetry, L_i and K_{sf} are expressed as:

$$\begin{aligned} L_{i,\parallel} &= \frac{\alpha_0}{2-\alpha_0} \qquad \alpha_0 = \frac{2}{\epsilon^2}\left[1 - \sqrt{1-\epsilon^2}\left(\frac{\sin^{-1}\epsilon}{\epsilon}\right)\right] \\ \epsilon &= \sqrt{1-h^2} \quad \text{(spheroid eccentricity)} \\ K_{sf,\parallel} &= \frac{8}{3}\left\{\frac{2h}{1-h^2} + \frac{2(1-2h^2)}{(1-h^2)^{3/2}} \tan^{-1}\left[\frac{(1-h^2)^{1/2}}{h}\right]\right\}^{-1} \end{aligned} \tag{A13}$$

For oblate spheroids oscillating perpendicularly to their axis of symmetry, L_i and K_{sf} are expressed as:

$$\begin{aligned} L_{i,\perp} &= \frac{\gamma_0}{2-\gamma_0} \qquad \gamma_0 = \frac{\sqrt{1-\epsilon^2}}{\epsilon^3} \sin^{-1}\epsilon - \left[\frac{1-\epsilon^2}{\epsilon^2}\right] \\ K_{sf,\perp} &= \frac{8}{3}\left\{ - \frac{h}{1-h^2} - \frac{2h^2-3}{(1-h^2)^{3/2}} \sin^{-1}(1-h^2)^{1/2}\right\}^{-1} \end{aligned} \tag{A14}$$

Richards et al. (2003) made the assumption of a random orientation of the particles and considered that two-third of the particles have their semi-major axis perpendicular to the direction of sound propagation, and one-third have their semi-major axis parallel to this direction. Thus:

$$\chi_{sv}(a') = \frac{2}{3}\chi_{sv,\perp}(a') + \frac{1}{3}\chi_{sv,\parallel}(a') \tag{A15}$$

where $\chi_{sv,\perp}$ and $\chi_{sv,\parallel}$ are the total normalized viscous cross-sections computed in the case of perpendicular and parallel orientation of the oblate spheroid in relation to the direction of sound propagation, respectively.

Acknowledgments

The authors wish to thank Alexis Buffet, Frédéric Lacroix and Fabien Thollet of INRAE technical staff for their assistance with the experimental work. Electron microscopy was

made at the Centre Technologique des Microstructures (CTμ) of the University of Lyon. This work was supported by the Compagnie Nationale du Rhône (CNR). Half of Adrien Vergne's PhD grant was funded by the CNR.

Data will be available on zenodo (zenodo link will be provided after acceptance of the paper).

References

Agrawal, Y. C., & Hanes, D. M. (2015). The implications of laser-diffraction measurements of sediment size distributions in a river to the potential use of acoustic backscatter for sediment measurements. *Water Resour. Res.*, *51*, 8854-8867.

Aleixo, R., Guerrero, M., Nones, M., & Ruther, N. (2020). Applying ADCPs for long-term monitoring of SSC in rivers. *Water Resour. Res.*, *56*.

Armijos, E., Crave, A., Espinoza, R., Fraizy, P., Dos Santos, A. L. M. R., Sampaio, F., ... Filizola, N. (2017). Measuring and modeling vertical gradients in suspended sediments in the Solimões/Amazon River. *Hydrological Processes*, *31*, 654-667.

Betteridge, K. F. E., Thorne, P. D., & Cook, R. D. (2008). Calibrating multi-frequency acoustic backscatter systems for studying near-bed suspended sediment transport processes. *Cont. Shelf Res.*, *28*, 227-235.

Burban, P.-Y., Lick, W., & Lick, J. (1989). The flocculation of fine-grained sediments in estuarine waters. *J. Geophys. Res. Oceans*, *94*, 8323-8330.

Downing, A., Thorne, P. D., & Vincent, C. E. (1995). Backscattering from a suspension in the near field of a piston transducer. *J. Acoust. Soc. Am.*, *97*, 1614-1620.

Droppo, I. G. (2001). Rethinking what constitutes suspended sediment. *Hydrological Processes*, *15*, 1551-1564.

Erdoğan, S., Garboczi, E. J., & Fowler, D. (2007). Shape and size of microfine aggregates: X-ray microcomputed tomography vs. laser diffraction. *Powder Technology*, *177*(2), 53–63.

Eshel, G., Levy, G. J., Mingelgrin, U., & Singer, M. J. (2004). Critical evaluation of the use of laser diffraction for particle-size distribution analysis. *Soil Sci. Soc. Am. J.*, *68*, 763-743.

François, R. E., & Garrison, G. R. (1982). Sound absorption based on ocean measurements: Part I: Pure water and magnesium sulfate contributions. *J. Acoust. Soc. Am.*, *75*, 896-907.

Gaunaurd, G. C., & Uberall, H. (1983). RST analysis of monostatic and bistatic acoustic echoes from an elastic sphere. *J. Acoust. Soc. Am.*, *73*, 1-12.

Gostiaux, L., & van Haren, H. (2010). Extracting meaningful information from uncalibrated backscattered echo intensity data. *J. Atmospheric Ocean. Technol.*, *27*, 943-949.

Gray, J. R., & Gartner, J. W. (2009). Technological advances in suspended-sediment surrogate monitoring. *Water Resour. Res.*, *45*, W00D29.

Guerrero, M., & Di Federico, V. (2018). Suspended sediment assessment by combining sound attenuation and backscatter measurements - analytical method and experimental validation. *Advances in Water Resources*, *113*, 167-179.

Hanes, D. M. (2012). On the possibility of single-frequency acoustic measurement of sand and clay concentrations in uniform suspensions. *Cont. Shelf Res.*, *46*, 64-66.

Haught, D., Venditti, J. G., & Wright, S. A. (2017). Calculation of in situ acoustic sediment attenuation using off-the-shelf horizontal ADCPs in low concentration settings. *Water Resour. Res.*, *53*, 5017-5037.

Hay, A. E. (1991). Sound scattering from a particle-laden, turbulent jet. *J. Acoust. Soc. Am.*, *90*, 2055-2074.

Hay, A. E., & Mercer, D. G. (1989). A note on the viscous attenuation of sound in suspensions. *J. Acoust. Soc. Am.*, *85*, 2215-2216.

Hay, A. E., & Sheng, J. (1992). Vertical profiles of suspended sand concentration and size from multifrequency acoustic backscatter. *J. Geophys. Res.*, *97*, 15661-15677.

Hunter, T. N., Darlison, L., Peakall, J., & Biggs, S. (2012). Using a multi-frequency acoustic backscatter system as an in situ high concentration dispersion monitor. *Chem. Eng. Sci.*, *80*, 409-418.

Hurther, D., Thorne, P. D., Bricault, M., Lemmin, U., & Barnoud, J.-M. (2011). A multi-frequency Acoustic Concentration and Velocity Profiler (ACVP) for boundary layer measurements of fine-scale flow and sediment transport processes. *Coast. Eng. J.*, *58*, 594-605.

Landers, M. N., Straub, T. D., Wood, M. S., & Domanski, M. M. (2016). *Sediment acoustic index method for computing continuous suspended-sediment concentrations.* USGS Techniques and Methods, book 3, chap. C5. Retrieved from `http://dx.doi.org/10.3133/tm3C5`

MacDonald, I. T., Vincent, C. E., Thorne, P. D., & Moate, B. D. (2013). Acoustic scattering from a suspension of flocculated sediments. *J. Geophys. Res.*, *118*, 2581-2594.

Masson, M., Angot, H., Le Boscond, C., Launay, M., Dabrin, A., Miège, C., ... Coquery, M. (2018). Sampling of suspended particulate matter using particle traps in the Rhône River: relevance and representativeness for the monitoring of contaminants. *Sci Total Environ.*, *637-638*, 538-549.

Medwin, H., & Clay, C. S. (1998). *Fundamentals of Acoustical Oceanography.* Academic Press.

Moate, B. D., & Thorne, P. D. (2012). Interpreting acoustic backscatter from suspended sediments of different and mixed mineralogical composition. *Cont. Shelf Res.*, *46*, 67-82.

Moore, S. A., Le Coz, J., Hurther, D., & Paquier, A. (2012). On the application of horizontal ADCPs to suspended sediment transport surveys in rivers. *Cont. Shelf Res.*, *46*, 50-63.

Moore, S. A., Le Coz, J., Paquier, A., & Hurther, D. (2013). Using multi-frequency acoustic attenuation to monitor grain size and concentration of suspended sediment in rivers. *J. Acoust. Soc. Am.*, *133*, 1959-1970.

Rice, H. P., Fairweather, M., Hunter, T. N., & Mahmoud, B. (2014). Measuring particle concentration in multiphase pipe flow using acoustic backscatter: Generalization of the dual-frequency inversion method. *J. Acoust. Soc. Am.*, *136*, 156-169.

Richards, S. D., Leighton, T. G., & Brown, N. R. (2003). Visco-inertial absorption in dilute suspensions of irregular particles. *Proceedings of the Royal Society of London*, *459*, 2153-2167.

Rouhnia, M., Keyvani, A., & Strom, K. (2014). Do changes in the size of mud flocs affect the acoustic backscatter values recorded by a Vector ADV? *Cont. Shelf Res.*, *84*, 84-92.

Schaafsma, A. S., & Hay, A. E. (1997). Attenuation in suspensions of irregularly shaped sediment particles: A two-parameter equivalent spherical scatter model. *J. Acoust. Soc. Am.*, *102*, 1485-1502.

Schjønning, P., McBride, R. A., Keller, T., & Obour, P. B. (2017). Predicting soil particle density from clay and soil organic matter contents. *Geoderma*, *286*, 83-87.

Sheng, J., & Hay, A. E. (1988). An examination of the spherical scatterer approximation in aquaeous suspensions of sand. *J. Acoust. Soc. Am.*, *83*, 598-610.

Sung, C. C., Huang, Y. J., Lai, J. S., & Hwang, G. W. (2008). Ultrasonic mea-

surement of suspended sediment concentrations: an experimental validation of the approach using kaolin suspensions and reservoir sediments under variable thermal conditions. *Hydrological Processes*, *22*, 3149-3154.

Szupiany, R., Lopez Weibel, C., Guerrero, M., Latosinski, F., Wood, M., Dominguez Ruben, L., & Oberg, K. (2019). Estimating sand concentrations using ADCP-based acoustic inversion in a large fluvial system characterized by bi-modal suspended-sediment distributions. *Earth Surface Processes and Landforms*, *44*, 1295-1308.

Thorne, P. D., & Buckingham, M. J. (2004). Measurements of scattering by suspensions of irregularly shaped sand particles and comparison with a single parameter modified sphere model. *J. Acoust. Soc. Am.*, *116*, 2876-2889.

Thorne, P. D., Hardcastle, P. J., & Soulsby, R. L. (1993). Analysis of acoustic measurements of suspended sediments. *J. Geophys. Res.*, *98*, 899-910.

Thorne, P. D., & Hurther, D. (2014). An overview on the use of backscattered sound for measuring suspended particle size and concentration profiles in non-cohesive inorganic sediment transport studies. *Cont. Shelf Res.*, *73*, 97-118.

Thorne, P. D., Hurther, D., & Moate, B. D. (2011). Acoustic inversions for measuring boundary layer suspended sediment processes. *J. Acoust. Soc. Am.*, *130*, 1188-1200.

Thorne, P. D., MacDonald, I. T., & Vincent, C. E. (2014). Modelling acoustic scattering by suspended flocculating sediments. *Cont. Shelf Res.*, *88*, 81-91.

Thorne, P. D., & Meral, R. (2008). Formulations for the scattering properties of suspended sandy sediments for use in the application of acoustics to sediment transport processes. *Cont. Shelf Res.*, *28*, 309-317.

Thosteson, E. D., & Hanes, D. M. (1998). A simplified method for determining sediment size and concentration from multiple frequency acoustic backscatter measurements. *J. Acoust. Soc. Am.*, *104*, 820-830.

Topping, D. J., & Wright, S. A. (2016). *Long-term continuous acoustical suspended-sediment measurements in rivers – Theory, application, bias, and error.* USGS Professional Paper 1823. Retrieved from `http://dx.doi.org/10.3133/pp1823`

Topping, D. J., Wright, S. A., Melis, T. S., & Rubin, D. M. (2007, August). High-resolution measurements of suspended-sediment concentration and grain size in the Colorado River in Grand Canyon using a multi-frequency acoustic system. In *Proceedings of the 10th international symposium on river sedimentation.* Russia, Moscow.

Urick, R. J. (1948). The absorption of sound in suspensions of irregular particles. *J. Acoust. Soc. Am.*, *20*, 283-289.

Venditti, J. G., Church, M., Attard, M. E., & Haught, D. (2016). Use of ADCPs for suspended sediment transport monitoring: an empirical approach. *Water Resour. Res.*, *52*, 2715-2736.

Vergne, A., Le Coz, J., Berni, C., & Pierrefeu, G. (2020). Using a Down-Looking Multifrequency ABS for Measuring Suspended Sediments in Rivers. *Water Resour. Res.*, *56*(2).

Vincent, C. E., & MacDonald, I. T. (2015). A flocculi model for the acoustic scattering from flocs. *Cont. Shelf Res.*, *104*, 15-24.

Wilson, G. W., & Hay, A. E. (2015). Acoustic backscatter inversion for suspended sediment concentration and size: A new approach using statistical inverse theory. *Cont. Shelf Res.*, *106*, 130-139.

Wright, S. A., Topping, D. J., & Williams, C. A. (2010, June). Discriminating silt-and-clay from suspended-sand in rivers using side-looking acoustic profilers. In *Proceedings of the 2nd joint federal interagency sedimentation conference.* USA, Las Vegas.